9

Nonlinear Adaptive Model Following Control for a 3-DOF Model Helicopter

Mitsuaki Ishitobi and Masatoshi Nishi
Department of Mechanical Systems Engineering
Kumamoto University
Japan

1. Introduction

Interest in designing feedback controllers for helicopters has increased over the last ten years or so due to the important potential applications of this area of research. The main difficulties in designing stable feedback controllers for helicopters arise from the nonlinearities and couplings of the dynamics of these aircraft. To date, various efforts have been directed to the development of effective nonlinear control strategies for helicopters (Sira-Ramirez *et al.*, 1994; Kaloust *et al.*, 1997; Kutay *et al.*, 2005; Avila *et al.*, 2003). Sira-Ramirez *et al.* applied dynamical sliding mode control to the altitude stabilization of a nonlinear helicopter model in vertical flight. Kaloust *et al.* developed a Lyapunov-based nonlinear robust control scheme for application to helicopters in vertical flight mode. Avila *et al.* derived a nonlinear 3-DOF (degree-of-freedom) model as a reduced-order model for a 7-DOF helicopter, and implemented a linearizing controller in an experimental system. Most of the existing results have concerned flight regulation.

This study considers the two-input, two-output nonlinear model following control of a 3-DOF model helicopter. Since the decoupling matrix is singular, a nonlinear structure algorithm (Shima *et al.*, 1997; Isurugi, 1990) is used to design the controller. Furthermore, since the model dynamics are described linearly by unknown system parameters, a parameter identification scheme is introduced in the closed-loop system.

Two parameter identification methods are discussed: The first method is based on the differential equation model. In experiments, it is found that this model has difficulties in obtaining a good tracking control performance, due to the inaccuracy of the estimated velocity and acceleration signals. The second parameter identification method is designed on the basis of a dynamics model derived by applying integral operators to the differential equations expressing the system dynamics. Hence this identification algorithm requires neither velocity nor acceleration signals. The experimental results for this second method show that it achieves better tracking objectives, although the results still suffer from tracking errors. Finally, we introduce additional terms into the equations of motion that express model uncertainties and external disturbances. The resultant experimental data show that the method constructed with the inclusion of these additional terms produces the best control performance.

2. System Description

Consider the tandem rotor model helicopter of Quanser Consulting, Inc. shown in Figs. 1 and 2. The helicopter body is mounted at the end of an arm and is free to move about the elevation, pitch and horizontal travel axes. Thus the helicopter has 3-DOF: the elevation ε, pitch θ and travel ϕ angles, all of which are measured via optical encoders. Two DC motors attached to propellers generate a driving force proportional to the voltage output of a controller.

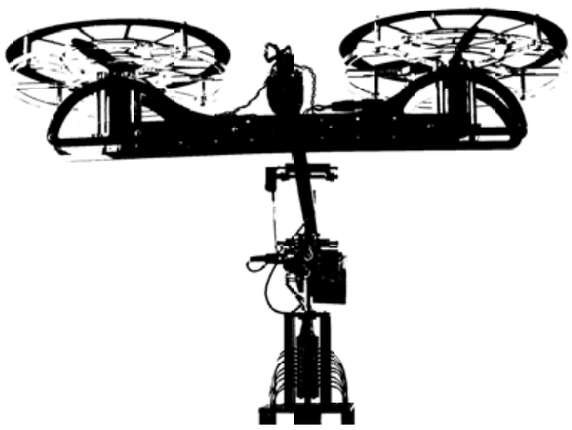

Fig. 1. Overview of the present model helicopter.

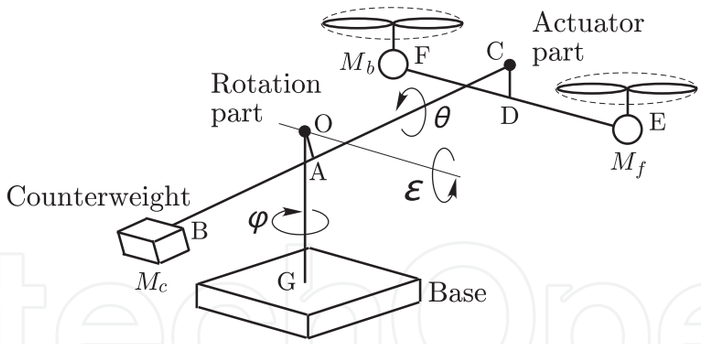

Fig. 2. Notation.

The equations of motion about axes ε, θ and ϕ are expressed as

$$\begin{aligned} J_\varepsilon \ddot{\varepsilon} &= -\left(M_f + M_b\right) g \frac{L_a}{\cos\delta_a} \cos\left(\varepsilon - \delta_a\right) + M_c g \frac{L_c}{\cos\delta_c} \cos\left(\varepsilon + \delta_c\right) - \eta_\varepsilon \dot{\varepsilon} \\ &\quad + K_m L_a \left(V_f + V_b\right) \cos\theta \end{aligned} \tag{1}$$

$$J_\theta \ddot{\theta} = -M_f g \frac{L_h}{\cos\delta_h} \cos\left(\theta - \delta_h\right) + M_b g \frac{L_h}{\cos\delta_h} \cos\left(\theta + \delta_h\right) - \eta_\theta \dot{\theta} + K_m L_h \left(V_f - V_b\right) \tag{2}$$

$$J_\phi \ddot{\phi} = -\eta_\phi \dot{\phi} - K_m L_a \left(V_f + V_b\right) \sin\theta. \tag{3}$$

A complete derivation of this model is presented in (Apkarian, 1998). The system dynamics are expressed by the following highly nonlinear and coupled state variable equations

$$\dot{\boldsymbol{x}}_p = f(\boldsymbol{x}_p) + [g_1(\boldsymbol{x}_p),\ g_2(\boldsymbol{x}_p)]\boldsymbol{u}_p \tag{4}$$

where

$$\begin{aligned}
\boldsymbol{x}_p &= [x_{p1},\ x_{p2},\ x_{p3},\ x_{p4},\ x_{p5},\ x_{p6}]^T \\
&= [\varepsilon,\ \dot{\varepsilon},\ \theta,\ \dot{\theta},\ \phi,\ \dot{\phi}]^T \\
\boldsymbol{u}_p &= [u_{p1},\ u_{p2}]^T \\
u_{p1} &= V_f + V_b \\
u_{p2} &= V_f - V_b \\
f(\boldsymbol{x}_p) &= \begin{bmatrix} \dot{\varepsilon} \\ p_1 \cos\varepsilon + p_2 \sin\varepsilon + p_3\dot{\varepsilon} \\ \dot{\theta} \\ p_5 \cos\theta + p_6 \sin\theta + p_7\dot{\theta} \\ \dot{\phi} \\ p_9\dot{\phi} \end{bmatrix} \\
g_1(\boldsymbol{x}_p) &= [0,\ p_4 \cos\theta,\ 0,\ 0,\ 0,\ p_{10} \sin\theta]^T \\
g_2(\boldsymbol{x}_p) &= [0,\ 0,\ 0,\ p_8,\ 0,\ 0]^T \\
p_1 &= \Big[-(M_f + M_b)gL_a + M_c g L_c\Big] \Big/ J_\varepsilon \\
p_2 &= -\Big[(M_f + M_b)gL_a \tan\delta_a + M_c g L_c \tan\delta_c\Big] \Big/ J_\varepsilon \\
p_3 &= -\eta_\varepsilon / J_\varepsilon \\
p_4 &= K_m L_a / J_\varepsilon \\
p_5 &= (-M_f + M_b)gL_h \Big/ J_\theta \\
p_6 &= -(M_f + M_b)gL_h \tan\delta_h \Big/ J_\theta \\
p_7 &= -\eta_\theta / J_\theta \\
p_8 &= K_m L_h / J_\theta \\
p_9 &= -\eta_\phi / J_\phi \\
p_{10} &= -K_m L_a / J_\phi \\
\delta_a &= \tan^{-1}\{(L_d + L_e)/L_a\} \\
\delta_c &= \tan^{-1}(L_d / L_c) \\
\delta_h &= \tan^{-1}(L_e / L_h)
\end{aligned}$$

The notation employed above is defined as follows: V_f, V_b [V]: Voltage applied to the front motor, voltage applied to the rear motor,
M_f, M_b [kg]: Mass of the front section of the helicopter, mass of the rear section,
M_c [kg]: Mass of the counterbalance,
L_d, L_c, L_a, L_e, L_h [m]: Distances OA, AB, AC, CD, DE=DF,
g [m/s^2]: gravitational acceleration,

J_ε, J_θ, J_ϕ [kg·m^2]: Moment of inertia about the elevation, pitch and travel axes,
η_ε, η_θ, η_ϕ [kg·m^2/s]: Coefficient of viscous friction about the elevation, pitch and travel axes.
The forces of the front and rear rotors are assumed to be F_f=$K_m V_f$ and F_b=$K_m V_b$ [N], respectively, where K_m [N/V] is a force constant. It may be noted that all the parameters p_i $(i = 1 \ldots 10)$ are constants. For the problem of the control of the position of the model helicopter, two angles, the elevation ε and the travel ϕ angles, are selected as the outputs from the three detected signals of the three angles. Hence, we have

$$\boldsymbol{y}_p = [\varepsilon,\ \phi]^T \tag{5}$$

3. Nonlinear Model Following Control

3.1 Control system design

In this section, a nonlinear model following control system is designed for the 3-DOF model helicopter described in the previous section.
First, the reference model is given as

$$\begin{cases} \dot{\boldsymbol{x}}_M = A_M \boldsymbol{x}_M + B_M \boldsymbol{u}_M \\ \boldsymbol{y}_M = C_M \boldsymbol{x}_M \end{cases} \tag{6}$$

where

$$\begin{aligned}
\boldsymbol{x}_M &= [x_{M1},\ x_{M2},\ x_{M3},\ x_{M4},\ x_{M5},\ x_{M6},\ x_{M7},\ x_{M8}]^T \\
\boldsymbol{y}_M &= [\varepsilon_M,\ \phi_M]^T \\
\boldsymbol{u}_M &= [u_{M1},\ u_{M2}]^T \\
A_M &= \begin{bmatrix} K_1 & 0 \\ 0 & K_2 \end{bmatrix} \\
K_i &= \begin{bmatrix} 0 & 1 & 0 & 0 \\ 0 & 0 & 1 & 0 \\ 0 & 0 & 0 & 1 \\ k_{i1} & k_{i2} & k_{i3} & k_{i4} \end{bmatrix},\ i = 1, 2 \\
B_M &= \begin{bmatrix} \boldsymbol{i}_1 & \boldsymbol{0} \\ \boldsymbol{0} & \boldsymbol{i}_1 \end{bmatrix} \\
C_M &= \begin{bmatrix} \boldsymbol{i}_2{}^T & \boldsymbol{0}^T \\ \boldsymbol{0}^T & \boldsymbol{i}_2{}^T \end{bmatrix} \\
\boldsymbol{i}_1 &= \begin{bmatrix} 0 \\ 0 \\ 0 \\ 1 \end{bmatrix},\ \boldsymbol{i}_2 = \begin{bmatrix} 1 \\ 0 \\ 0 \\ 0 \end{bmatrix}
\end{aligned}$$

From (4) and (6), the augmented state equation is defined as follows.

$$\dot{\boldsymbol{x}} = f(\boldsymbol{x}) + G(\boldsymbol{x})\boldsymbol{u} \tag{7}$$

where

$$\begin{aligned} \boldsymbol{x} &= [\boldsymbol{x}_p^T,\ \boldsymbol{x}_M^T]^T \\ \boldsymbol{u} &= [\boldsymbol{u}_p^T,\ \boldsymbol{u}_M^T]^T \\ f(\boldsymbol{x}) &= \begin{bmatrix} f(\boldsymbol{x}_p) \\ A_M \boldsymbol{x}_M \end{bmatrix} \\ G(\boldsymbol{x}) &= \begin{bmatrix} g_1(\boldsymbol{x}_p) & g_2(\boldsymbol{x}_p) & O \\ \mathbf{0} & \mathbf{0} & B_M \end{bmatrix} \end{aligned}$$

Here, we apply a nonlinear structure algorithm to design a model following controller (Shima *et al.*, 1997; Isurugi, 1990). New variables and parameters in the following algorithm are defined below the input (19).

- Step 1

The tracking error vector is given by

$$\boldsymbol{e} = \begin{bmatrix} e_1 \\ e_2 \end{bmatrix} = \begin{bmatrix} x_{M1} - x_{p1} \\ x_{M5} - x_{p5} \end{bmatrix} \tag{8}$$

Differentiating the tracking error (8) yields

$$\begin{aligned} \dot{\boldsymbol{e}} &= \frac{\partial \boldsymbol{e}}{\partial \boldsymbol{x}} \{f(\boldsymbol{x}) + G(\boldsymbol{x})\boldsymbol{u}\} \\ &= \begin{bmatrix} -x_{p2} + x_{M2} \\ -x_{p6} + x_{M6} \end{bmatrix} \end{aligned} \tag{9}$$

Since the inputs do not appear in (9), we proceed to step 2.

- Step 2

Differentiating (9) leads to

$$\ddot{\boldsymbol{e}} = \frac{\partial \dot{\boldsymbol{e}}}{\partial \boldsymbol{x}} \{f(\boldsymbol{x}) + G(\boldsymbol{x})\boldsymbol{u}\} \tag{10}$$

$$= \begin{bmatrix} r_1(\boldsymbol{x}) \\ -p_9 x_{p6} + x_{M7} \end{bmatrix} + [B_u(\boldsymbol{x}),\ B_r(\boldsymbol{x})]\,\boldsymbol{u} \tag{11}$$

where

$$B_u(\boldsymbol{x}) = \begin{bmatrix} -p_4 \cos x_{p3} & 0 \\ -p_{10} \sin x_{p3} & 0 \end{bmatrix},\ B_r(\boldsymbol{x}) = O$$

From (11), the decoupling matrix $B_u(\boldsymbol{x})$ is obviously singular. Hence, this system is not decouplable by static state feedback. The equation (11) can be re-expressed as

$$\ddot{e}_1 = r_1(\boldsymbol{x}) - p_4 \cos x_{p3} u_{p1} \tag{12}$$

$$\ddot{e}_2 = -p_9 x_{p6} + x_{M7} - p_{10} \sin x_{p3} u_{p1} \tag{13}$$

then, by eliminating u_{p1} from (13) using (12) under the assumption of $u_{p1} \neq 0$, we obtain

$$\ddot{e}_2 = -p_9 x_{p6} + x_{M7} + \frac{p_{10}}{p_4} \tan x_{p3} (\ddot{e}_1 - r_1(\boldsymbol{x})) \tag{14}$$

- Step 3

Further differentiating (14) gives rise to

$$\begin{aligned} e_2^{(3)} &= \frac{\partial \ddot{e}_2}{\partial \boldsymbol{x}} \left\{ f(\boldsymbol{x}) + G(\boldsymbol{x})\boldsymbol{u} \right\} + \frac{\partial \ddot{e}_2}{\partial \ddot{e}_1} e_1^{(3)} \\ &= \frac{p_{10}}{p_4} \tan x_{p3} \left\{ -x_{p2} \left(p_1 \sin x_{p1} - p_2 \cos x_{p1} \right) + p_3 (x_{M3} - r_1(\boldsymbol{x})) - x_{M4} + e_1^{(3)} \right\} \\ &\quad - \frac{p_{10}}{p_4 \cos x_{p3}} x_{p4} \left(\ddot{e}_1 - r_1(\boldsymbol{x}) \right) - p_9^2 x_{p6} + x_{M8} \\ &\quad + \left[p_{10} \sin x_{p3} (p_3 - p_9),\ 0,\ 0,\ 0 \right] \boldsymbol{u} \end{aligned} \tag{15}$$

As well as step 2, we eliminate u_{p1} from (15) using (12), and it is obtained that

$$\begin{aligned} e_2^{(3)} &= \frac{p_{10}}{p_4} \tan x_{p3} \left\{ p_3 x_{M3} - x_{p2} \left(p_1 \sin x_{p1} - p_2 \cos x_{p1} \right) - p_3 r_1(\boldsymbol{x}) - x_{M4} + e_1^{(3)} \right. \\ &\quad \left. - (p_3 - p_9) \left(\ddot{e}_1 - r_1(\boldsymbol{x}) \right) \right\} + x_{M8} - p_9^2 x_{p6} - \frac{p_{10}}{p_4 \cos x_{p3}} x_{p4} \left(\ddot{e}_1 - r_1(\boldsymbol{x}) \right) \end{aligned} \tag{16}$$

- Step 4

It follows from the same operation as step 3 that

$$\begin{aligned} e_2^{(4)} &= \frac{\partial e_2^{(3)}}{\partial \boldsymbol{x}} \left\{ f(\boldsymbol{x}) + G(\boldsymbol{x})\boldsymbol{u}_x \right\} + \frac{\partial e_2^{(3)}}{\partial \ddot{e}_1} e_1^{(3)} + \frac{\partial e_2^{(3)}}{\partial e_1^{(3)}} e_1^{(4)} \\ &= r_2(\boldsymbol{x}) + \left[d_1(\boldsymbol{x}),\ d_2(\boldsymbol{x}),\ d_3(\boldsymbol{x}),\ 1 \right] \boldsymbol{u} \end{aligned} \tag{17}$$

From (12) and (17), we obtain

$$\begin{bmatrix} e_1^{(2)} \\ e_2^{(4)} \end{bmatrix} = \begin{bmatrix} r_1(\boldsymbol{x}) \\ r_2(\boldsymbol{x}) \end{bmatrix} + \begin{bmatrix} -p_4 \cos x_{p3} & 0 & 0 & 0 \\ d_1(\boldsymbol{x}) & d_2(\boldsymbol{x}) & d_3(\boldsymbol{x}) & 1 \end{bmatrix} \boldsymbol{u}_M \tag{18}$$

The system is input-output linearizable and the model following input vector is determined by

$$\boldsymbol{u}_p = R(\boldsymbol{x}) + S(\boldsymbol{x})\, \boldsymbol{u}_M \tag{19}$$

$$\begin{aligned} R(\boldsymbol{x}) &= \frac{1}{d_2(\boldsymbol{x}) p_4 \cos x_{p3}} \begin{bmatrix} -d_2(\boldsymbol{x}) & 0 \\ d_1(\boldsymbol{x}) & p_4 \cos x_{p3} \end{bmatrix} \begin{bmatrix} \bar{e}_1 - r_1(\boldsymbol{x}) \\ \bar{e}_2 - r_2(\boldsymbol{x}) \end{bmatrix} \\ S(\boldsymbol{x}) &= \frac{-1}{d_2(\boldsymbol{x}) p_4 \cos x_{p3}} \begin{bmatrix} -d_2(\boldsymbol{x}) & 0 \\ d_1(\boldsymbol{x}) & p_4 \cos x_{p3} \end{bmatrix} \begin{bmatrix} 0 & 0 \\ d_3(\boldsymbol{x}) & 1 \end{bmatrix} \end{aligned}$$

where

$$
\begin{aligned}
\bar{e}_1 &= -\sigma_{12}\dot{e}_1 - \sigma_{11}e_1 \\
\bar{e}_2 &= -\sigma_{24}e_2^{(3)} - \sigma_{23}\ddot{e}_2 - \sigma_{22}\dot{e}_2 - \sigma_{21}e_2 \\
r_1(\boldsymbol{x}) &= -p_1\cos x_{p1} - p_2\sin x_{p1} - p_3 x_{p2} + x_{M3} \\
r_2(\boldsymbol{x}) &= \left\{ -\left(p_1\sin x_{p1} - p_2\cos x_{p1}\right)\left(\frac{p_9 p_{10}}{p_4}\tan x_{p3} + \frac{p_{10}}{p_4\cos x_{p3}}x_{p4}\right)\right. \\
&\quad \left. -\frac{p_{10}}{p_4}x_{p2}\tan x_{p3}\left(p_1\cos x_{p1} + p_2\sin x_{p1}\right)\right\} x_{p2} \\
&\quad + \left\{ \frac{p_3 p_{10}}{p_4\cos x_{p3}}x_{p4} + \frac{p_{10}}{p_4}\tan x_{p3}\left(p_3 p_9 - p_1\sin x_{p1} + p_2\cos x_{p1}\right)\right\}\left(x_{M3} - r_1(\boldsymbol{x})\right) \\
&\quad + \left\{ p_3\left(x_{M3} - r_1(\boldsymbol{x})\right) + \left(2x_{p4}\tan x_{p3} - p_3 + p_9\right)\left(\ddot{e}_1 - r_1(\boldsymbol{x})\right)\right. \\
&\quad \left. - x_{M4} + e_1^{(3)} - x_{p2}\left(p_1\sin x_{p1} - p_2\cos x_{p1}\right)\right\}\frac{p_{10}}{p_4\cos x_{p3}}x_{p4} \\
&\quad + \frac{p_{10}}{p_4\cos x_{p3}}\left(\ddot{e}_1 - r_1(\boldsymbol{x})\right)\left(p_5\cos x_{p3} + p_6\sin x_{p3} + p_7 x_{p4}\right) \\
&\quad + \left\{ \frac{p_{10}}{p_4\cos x_{p3}}x_{p4} - \frac{p_{10}}{p_4}\left(p_3 - p_9\right)\tan x_{p3}\right\} e_1^{(3)} \\
&\quad + \frac{p_{10}}{p_4}\tan x_{p3}\left\{\left(p_3 - p_9\right)x_{M4} - k_1 x_{M1} - k_2 x_{M2} - k_3 x_{M3} - k_4 x_{M4}\right\} \\
&\quad - \frac{p_{10}}{p_4\cos x_{p3}}x_{p4}x_{M4} + k_5 x_{M5} + k_6 x_{M6} + k_7 x_{M7} + k_8 x_{M8} + \frac{p_{10}}{p_4}e_1^{(4)}\tan x_{p3} - p_9^3 x_{p6} \\
d_1(\boldsymbol{x}) &= \left(p_3 p_9 - p_1\sin x_{p1} + p_2\cos x_{p1} - p_9^2\right)p_{10}\sin x_{p3} + \frac{p_3 p_{10}}{\cos x_{p3}} \\
d_2(\boldsymbol{x}) &= \frac{p_8 p_{10}}{p_4\cos x_{p3}}\left(\ddot{e}_1 - r_1(\boldsymbol{x})\right) \\
d_3(\boldsymbol{x}) &= -\frac{p_{10}}{p_4}\tan x_{p3} \\
e_1 &= x_{M1} - x_{p1} \\
\dot{e}_1 &= x_{M2} - x_{p2} \\
\ddot{e}_1 &= -\sigma_{12}\dot{e}_1 - \sigma_{11}e_1 \\
e_1^{(3)} &= (\sigma_{12}^2 - \sigma_{11})\dot{e}_1 + \sigma_{12}\sigma_{11}e_1 \\
e_1^{(4)} &= (-\sigma_{12}^3 + 2\sigma_{12}\sigma_{11})\dot{e}_1 - \sigma_{11}(\sigma_{12}^2 - \sigma_{11})e_1 \\
e_2 &= x_{M5} - x_{p5} \\
\dot{e}_2 &= x_{M6} - x_{p6} \\
\ddot{e}_2 &= \frac{p_{10}}{p_4}\tan x_{p3}\left(\ddot{e}_1 - r_1(\boldsymbol{x})\right) - p_9 x_{p6} + x_{M7} \\
e_2^{(3)} &= \frac{p_{10}}{p_4}\tan x_{p3}\left\{ p_3\left(x_{M3} - r_1(\boldsymbol{x})\right) - x_{p2}\left(p_1\sin x_{p1} - p_2\cos x_{p1}\right)\right. \\
&\quad \left. + e_1^{(3)} + \left(p_3 - p_9\right)\left(r_1(\boldsymbol{x}) - \ddot{e}_1\right) - x_{M4}\right\} + x_{M8} + \frac{p_{10}}{p_4\cos x_{p3}}x_{p4}\left(\ddot{e}_1 - r_1(\boldsymbol{x})\right) - p_9^2 x_{p_6}
\end{aligned}
$$

The input vector is always available since the term $d_2(\boldsymbol{x})\cos x_{p3}$ does not vanish for $-\pi/2 < \theta < \pi/2$. The design parameters $\sigma_{ij}\quad (i = 1,2, j = 1,\cdots,4)$ are selected so that the following characteristic equations are stable.

$$\lambda^2 + \sigma_{12}\lambda + \sigma_{11} = 0 \tag{20}$$

$$\lambda^4 + \sigma_{24}\lambda^3 + \sigma_{23}\lambda^2 + \sigma_{22}\lambda + \sigma_{21} = 0 \tag{21}$$

Then, the closed-loop system has the following error equations

$$\ddot{e}_1 + \sigma_{12}\dot{e}_1 + \sigma_{11}e_1 = 0 \tag{22}$$

$$e_2^{(4)} + \sigma_{24}e_2^{(3)} + \sigma_{23}\ddot{e}_2 + \sigma_{22}\dot{e}_2 + \sigma_{21}e_2 = 0 \tag{23}$$

and the plant outputs converge to the reference outputs. From (11) and (17), u_{p1} and u_{p2} appear first in $\ddot{e}_1$ and $e_2^{(4)}$, respectively. Thus, there are no zero dynamics and the system is minimum phase since the order of (4) is six. Further, we can see that the order of the reference model should be eight so that the inputs (19) do not include the derivatives of the reference inputs $\boldsymbol{u}_M$.

Since the controller requires the angular velocity signals $\dot{\varepsilon}$, $\dot{\theta}$ and $\dot{\phi}$, in the experiment these signals are calculated numerically from the measured angular positions by a discretized differentiator with the first-order filter

$$H_l(z) = \frac{\alpha\left(1 - z^{-1}\right)}{1 - z^{-1} + \alpha T_s} \tag{24}$$

which is derived by substituting

$$s = \frac{(1 - z^{-1})}{T_s} \tag{25}$$

into the differentiator

$$G_l(s) = \frac{\alpha s}{s + \alpha} \tag{26}$$

where z^{-1} is a one-step delay operator, T_s is the sampling period and the design parameter α is a positive constant. Hence, for example, we have

$$\dot{\varepsilon}(k) \approx \frac{1}{\alpha T_s + 1}\left[\dot{\varepsilon}(k-1) + \alpha\left\{\varepsilon(k) - \varepsilon(k-1)\right\}\right]$$

$$\ddot{\varepsilon}(k) \approx \frac{1}{\alpha T_s + 1}\left[\ddot{\varepsilon}(k-1) + \alpha\left\{\dot{\varepsilon}(k) - \varepsilon(k-1)\right\}\right]$$

$$\dot{\theta}(k) \approx \frac{1}{\alpha T_s + 1}\left[\dot{\theta}(k-1) + \alpha\left\{\theta(k) - \theta(k-1)\right\}\right]$$

$$\ddot{\theta}(k) \approx \frac{1}{\alpha T_s + 1}\left[\ddot{\theta}(k-1) + \alpha\left\{\dot{\theta}(k) - \theta(k-1)\right\}\right]$$

$$\dot{\phi}(k) \approx \frac{1}{\alpha T_s + 1}\left[\dot{\phi}(k-1) + \alpha\left\{\phi(k) - \phi(k-1)\right\}\right]$$

$$\ddot{\phi}(k) \approx \frac{1}{\alpha T_s + 1}\left[\ddot{\phi}(k-1) + \alpha\left\{\dot{\phi}(k) - \phi(k-1)\right\}\right]$$

3.2 Experimental studies

The control algorithm described above was applied to the experimental system shown in Section 2. The nominal values of the physical constants are as follows: J_ε=0.86 [kg·m^2], J_θ=0.044 [kg·m^2], J_ϕ=0.82 [kg·m^2], L_a=0.62 [m], L_c=0.44 [m], L_d=0.05 [m], L_e=0.02 [m], L_h=0.177 [m], M_f=0.69 [kg], M_b=0.69 [kg], M_c=1.67 [kg], K_m=0.5 [N/V], g=9.81 [m/s^2], η_ε=0.001 [kg·m^2/s], η_θ=0.001 [kg·m^2/s], η_ϕ=0.005 [kg·m^2/s].

The design parameters are given as follows: The sampling period of the inputs and the outputs is set as $T_s = 2$ [ms]. The inputs u_{M1} and u_{M2} of the reference model are given by

$$u_{M1} = \begin{cases} 0.3, & 45k - 30 \le t < 45k - 7.5 \\ -0.1, & 45k - 7.5 \le t < 45k + 15 \end{cases}$$
$$u_{M2} = \begin{cases} 0, & 0 \le t < 7.5 \\ 0.4, & 45k - 37.5 \le t < 45k - 22.5 \\ -0.4, & 45k - 22.5 \le t < 45k \end{cases} \quad (27)$$
$$k = 0, 1, 2, \cdots$$

All the eigenvalues of the matrices K_1 and K_2 are -1, and the characteristic roots of the error equations (22) and (23) are specified as $(-2.0,\ -3.0)$ and $(-2.0,\ -2.2,\ -2.4,\ -2.6)$, respectively. The origin of the elevation angle ε is set as a nearly horizontal level, so the initial angle is $\varepsilon = -0.336$ when the voltages of two motors are zero, i.e., $V_f = V_b = 0$.

The outputs of the experimental results are shown in Figs. 3 and 4. The tracking is incomplete since there are parameter uncertainties in the model dynamics.

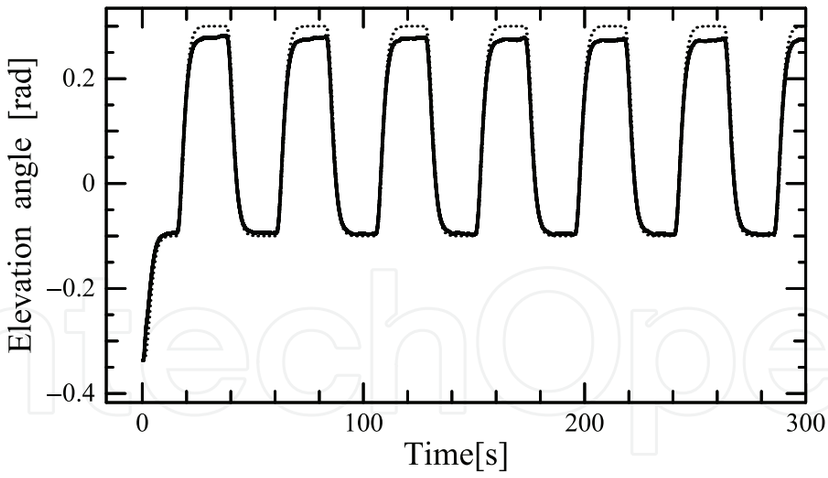

Fig. 3. Time evolution of angle ε (—) and reference output ε_M ($\cdots$).

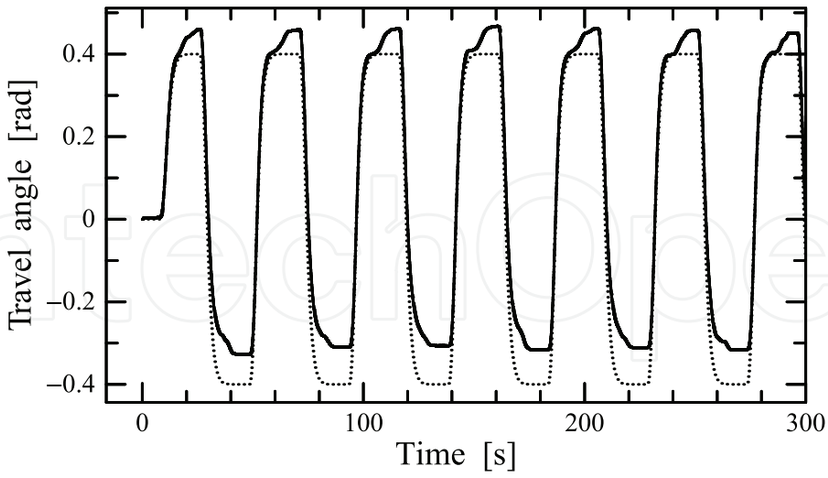

Fig. 4. Time evolution of angle ϕ (—) and reference output ϕ_M ($\cdots$).

4. Parameter Identification Based on the Differential Equations

4.1 Parameter identification algorithm

It is difficult to obtain the desired control performance by applying the algorithm in the previous section directly to the experimental system, since there are parameter uncertainties in the model dynamics. However, it is straightforward to see that the system dynamics (4) are linear with respect to unknown parameters, even though the equations are nonlinear. It is therefore possible to introduce a parameter identification scheme in the feedback control loop. In the present study, the parameter identification scheme is designed in discrete-time form using measured discrete-time signals. Hence, the estimated parameters are calculated recursively at every instant kT, where T is the updating period of the parameters and k is a nonnegative integer. Henceforth we omit T for simplicity. Then, the dynamics of the model helicopter given by equation (4) can be re-expressed as

$$\begin{aligned} w_1(k) &\equiv \ddot{\varepsilon}(k) \\ &= \boldsymbol{\zeta}_1^T \boldsymbol{v}_1(k) \end{aligned} \tag{28}$$

$$\begin{aligned} w_2(k) &\equiv \ddot{\theta}(k) \\ &= \boldsymbol{\zeta}_2^T \boldsymbol{v}_2(k) \end{aligned} \tag{29}$$

$$\begin{aligned} w_3(k) &\equiv \ddot{\phi}(k) \\ &= \boldsymbol{\zeta}_3^T \boldsymbol{v}_3(k) \end{aligned} \tag{30}$$

where

$$\begin{aligned}
\boldsymbol{\zeta}_1 &= [p_1,\ p_2,\ p_3,\ p_4]^T \\
\boldsymbol{\zeta}_2 &= [p_5,\ p_6,\ p_7,\ p_8]^T \\
\boldsymbol{\zeta}_3 &= [p_9,\ p_{10}]^T \\
\boldsymbol{v}_1(k) &= [v_{11}(k),\ v_{12}(k),\ v_{13}(k),\ v_{14}(k)]^T \\
\boldsymbol{v}_2(k) &= [v_{21}(k),\ v_{22}(k),\ v_{23}(k),\ v_{24}(k)]^T \\
\boldsymbol{v}_3(k) &= [v_{31}(k),\ v_{32}(k)]^T \\
v_{11}(k) &= \cos\varepsilon(k),\ v_{12}(k) = \sin\varepsilon(k) \\
v_{13}(k) &= \dot{\varepsilon}(k),\ v_{14}(k) = u_{p1}\cos\theta(k) \\
v_{21}(k) &= \cos\theta(k),\ v_{22}(k) = \sin\theta(k) \\
v_{23}(k) &= \dot{\theta}(k),\ v_{24}(k) = u_{p2}(k) \\
v_{31}(k) &= \dot{\phi}(k),\ v_{32}(k) = u_{p1}\sin\theta(k)
\end{aligned}$$

Defining the estimated parameter vectors corresponding to the vectors $\boldsymbol{\zeta}_1,\ \boldsymbol{\zeta}_2,\ \boldsymbol{\zeta}_3$ as $\widehat{\boldsymbol{\zeta}}_1(k)$, $\widehat{\boldsymbol{\zeta}}_2(k), \widehat{\boldsymbol{\zeta}}_3(k)$, the estimated values of $w_1(k),\ w_2(k),\ w_3(k)$ are obtained as

$$\widehat{w}_1(k) = \widehat{\boldsymbol{\zeta}}_1^T(k)\boldsymbol{v}_1(k) \tag{31}$$

$$\widehat{w}_2(k) = \widehat{\boldsymbol{\zeta}}_2^T(k)\boldsymbol{v}_2(k) \tag{32}$$

$$\widehat{w}_3(k) = \widehat{\boldsymbol{\zeta}}_3^T(k)\boldsymbol{v}_3(k) \tag{33}$$

respectively.
Along with the angular velocities, the angular accelerations $w_1(k) = \ddot{\varepsilon}(k)$, $w_2(k) = \ddot{\theta}(k)$, $w_3(k) = \ddot{\phi}(k)$ are also obtained by numerical calculation using a discretized differentiator.

The parameters are estimated using a recursive least squares algorithm as follows.

$$\begin{aligned}
\widehat{\boldsymbol{\zeta}}_i(k) &= \widehat{\boldsymbol{\zeta}}_i(k-1) + \frac{P_i(k-1)\boldsymbol{v}_i(k-1)\left[w_i(k-1) - \widehat{w}_i(k-1)\right]}{\lambda_i + \boldsymbol{v}_i^T(k-1)P_i(k-1)\boldsymbol{v}_i(k-1)} \\
P_i^{-1}(k) &= \lambda_i P_i^{-1}(k-1) + \boldsymbol{v}_i(k-1)\boldsymbol{v}_i^T(k-1) \\
P_i^{-1}(0) &> 0,\quad 0 < \lambda_i \leq 1,\ i = 1, 2, 3
\end{aligned} \tag{34}$$

Then, the tracking of the two outputs is achieved under the persistent excitation of the signals $\boldsymbol{v}_i, i = 1, 2, 3$.

4.2 Experimental studies

The estimation and control algorithm described above was applied to the experimental system shown in Section 2.
The design parameters are given as follows: The sampling period of the inputs and the outputs is set as $T_s = 2$ [ms] and the updating period of the parameters, T, takes the same value,

$T = 2$ [ms]. Further, the filter parameter, α, for the estimation of velocities and accelerations is $\alpha = 100$. The variation ranges of the identified parameters are restricted as

$$\begin{aligned} -1.8 \le \widehat{p}_1 \le -0.8, \qquad & -2.2 \le \widehat{p}_2 \le -1.2 \\ -0.3 \le \widehat{p}_3 \le 0.0, \qquad & 0.1 \le \widehat{p}_4 \le 0.6 \\ -0.5 \le \widehat{p}_5 \le 0.5, \qquad & -7.0 \le \widehat{p}_6 \le -5.2 \\ -0.6 \le \widehat{p}_7 \le 0.0, \qquad & 1.5 \le \widehat{p}_8 \le 2.2 \\ -0.5 \le \widehat{p}_9 \le 0.0, \qquad & -0.5 \le \widehat{p}_{10} \le -0.1 \end{aligned} \tag{35}$$

The design parameters of the identification algorithm are fixed at the values $\lambda_1 = 0.999$, $\lambda_2 = 0.9999$, $\lambda_3 = 0.999$ and ${P_1}^{-1}(0) = {P_2}^{-1}(0) = 10^4 I_4$, ${P_3}^{-1}(0) = 10^4 I_2$. The other design parameters are the same as those of the previous section. The values of the design parameters above are chosen by mainly trial and error. The selection of the sampling period is most important. The achievable minimum sampling period is 2 [ms] due to the calculation ability of the computer. The longer it is, the worse the tracking control performance is.
The outputs of the experimental results are shown in Figs. 5 and 6. The tracking is incomplete because the neither of the output errors of ε or ϕ converge. Figures 7, 8 and 9 display the estimated parameters. All of the estimated parameters move to the limiting values of the variation range.

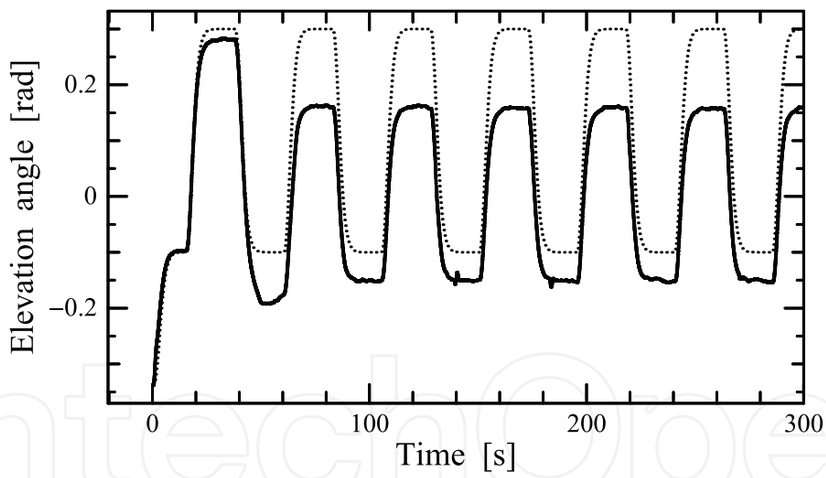

Fig. 5. Time evolution of angle ε (—) and reference output ε_M ($\cdots$).

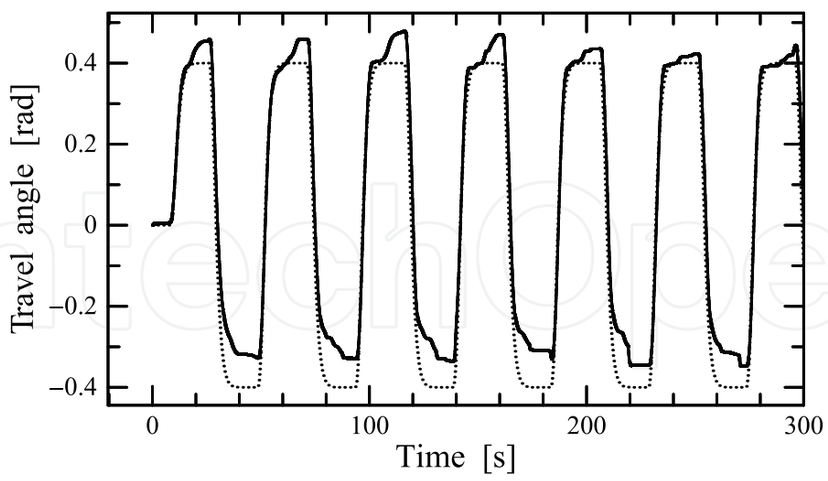

Fig. 6. Time evolution of angle ϕ (—) and reference output ϕ_M $(\cdots)$.

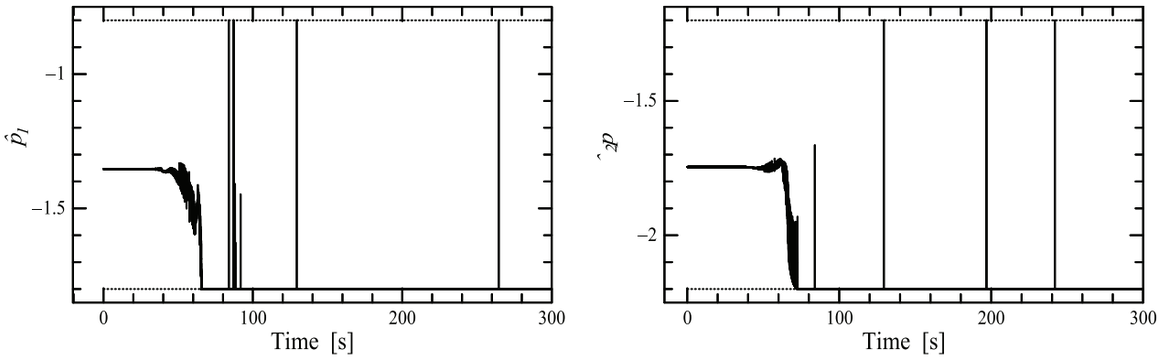

Fig. 7. Time evolution of the estimated parameters $\hat{p}_1$ and $\hat{p}_2$. The dotted lines represent the limited values of variation.

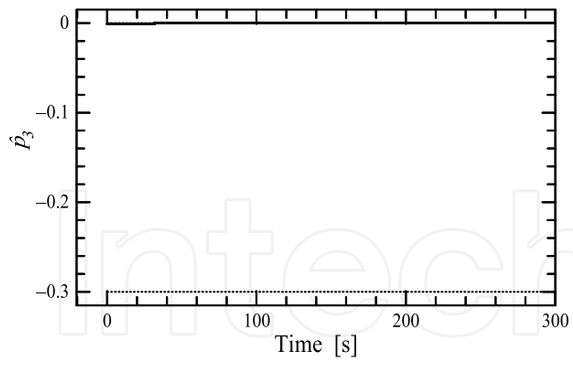
$\hat{p}_3$
0
−0.1
−0.2
−0.3
0
100
200
300
Time [s]

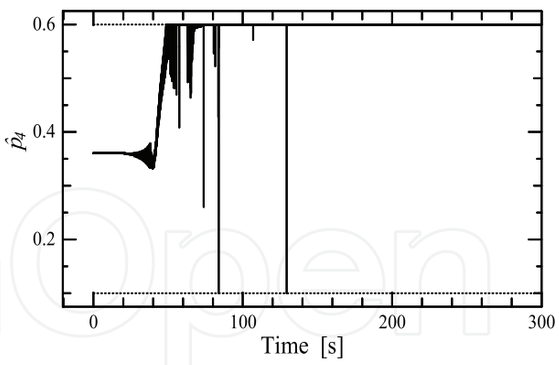
$\hat{p}_4$
0.6
0.4
0.2
0
100
200
300
Time [s]

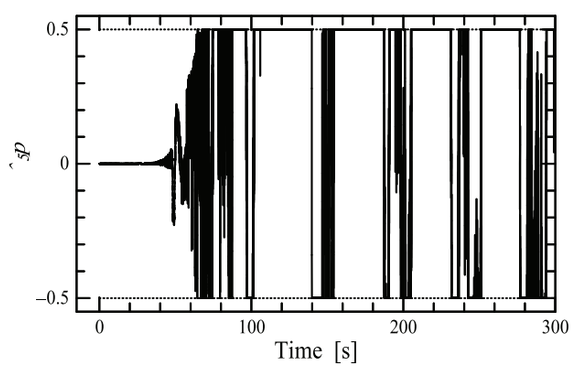
$\hat{p}_5$
0.5
0
−0.5
0
100
200
300
Time [s]

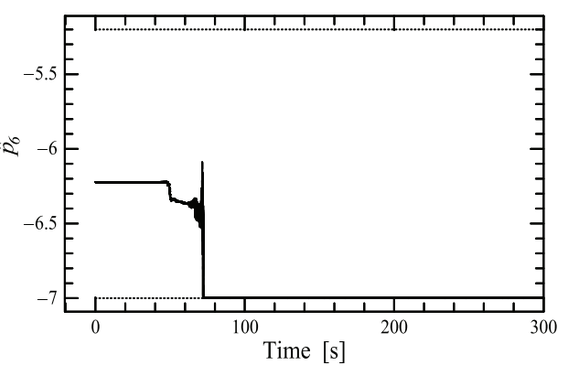
$\hat{p}_6$
−5.5
−6
−6.5
−7
0
100
200
300
Time [s]

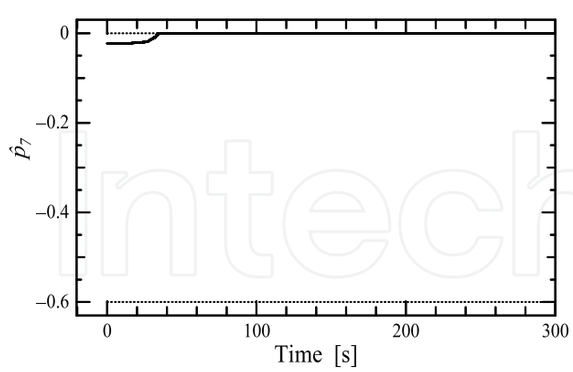
$\hat{p}_7$
0
−0.2
−0.4
−0.6
0
100
200
300
Time [s]

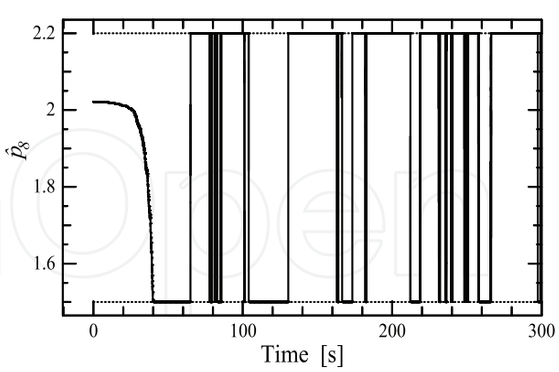
$\hat{p}_8$
2.2
2
1.8
1.6
0
100
200
300
Time [s]

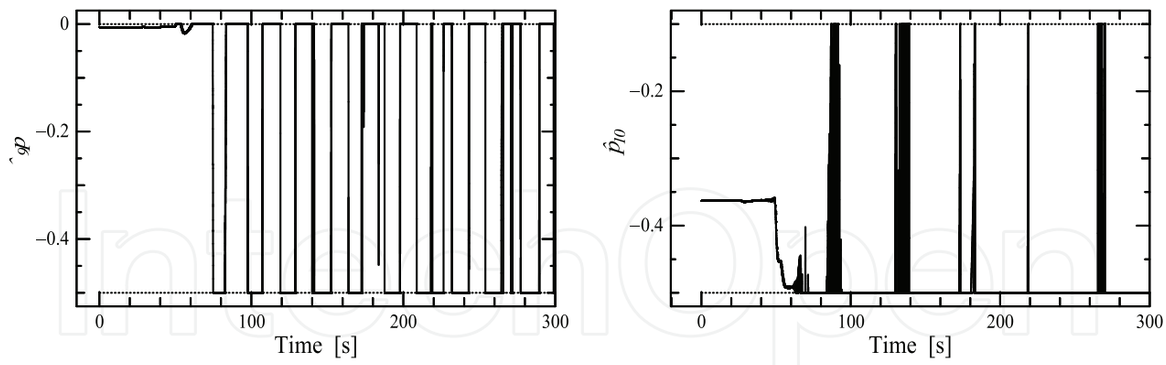

Fig. 8. Time evolution of the estimated parameters from $\hat{p}_3$ to $\hat{p}_{10}$. The dotted lines represent the limited values of variation.

5. Parameter Identification Based on the Integral Form of the Model Equations

5.1 The model equations without model uncertainties and external disturbances

5.1.1 Parameter identification algorithm

The main reason why the experimental results exhibit the poor tracking performance described in the previous subsection 4.2 lies in the fact that the parameter identification is unsatisfactory due to the inaccuracy of the estimation of the velocity and the acceleration signals. To overcome this problem, a parameter estimation scheme is designed for modified dynamics equations obtained by applying integral operators to the differential equations expressing the system dynamics (28)-(30) in this subsection. Neither velocities nor accelerations appear in these modified equations. Define $z_1(k)$ by the following double integral

$$z_1(k) \equiv \int_{kT-nT}^{kT} \int_{\tau-nT}^{\tau} \ddot{\varepsilon}(\sigma) d\sigma d\tau \tag{36}$$

Then, the direct calculation of the right-hand side of equation (36) leads to

$$\begin{aligned} \int_{kT-nT}^{kT} \int_{\tau-nT}^{\tau} \ddot{\varepsilon}(\sigma) d\sigma d\tau &= \int_{kT-nT}^{kT} \left(\dot{\varepsilon}(\tau) - \dot{\varepsilon}(\tau - nT)\right) d\tau \\ &= \varepsilon(kT) - 2\varepsilon(kT - nT) + \varepsilon(kT - 2nT) \end{aligned} \tag{37}$$

Next, discretizing the double integral of the right-hand side of equation (28) yields

$$\begin{aligned} & p_1 \int_{kT-nT}^{kT} \int_{\tau-nT}^{\tau} \cos\varepsilon(\sigma) d\sigma d\tau + \cdots + p_3 \int_{kT-nT}^{kT} \{\varepsilon(\tau) - \varepsilon(\tau - nT)\} d\tau + \cdots \\ & \approx p_1 T^2 \sum_{l=k-(n-1)}^{k} \sum_{i=l-(n-1)}^{l} \cos\varepsilon(i) + \cdots + p_3 T \sum_{l=k-(n-1)}^{k} \{\varepsilon(l) - \varepsilon(l - (n-1))\} + \cdots \end{aligned} \tag{38}$$

As a result, the integral form of the dynamics is obtained as

$$z_i(k) = \zeta_i^T \bar{v}_i(k),\ i = 1,\ 2,\ 3 \tag{39}$$

where

$$z_1(k) \equiv \varepsilon(k) - 2\varepsilon(k-n) + \varepsilon(k-2n) \tag{40}$$
$$z_2(k) \equiv \theta(k) - 2\theta(k-n) + \theta(k-2n) \tag{41}$$
$$z_3(k) \equiv \phi(k) - 2\phi(k-n) + \phi(k-2n) \tag{42}$$
$$\bar{\boldsymbol{v}}_1(k) = [\bar{v}_{11}(k),\ \bar{v}_{12}(k),\ \bar{v}_{13}(k),\ \bar{v}_{14}(k)]^T$$
$$\bar{\boldsymbol{v}}_2(k) = [\bar{v}_{21}(k),\ \bar{v}_{22}(k),\ \bar{v}_{23}(k),\ \bar{v}_{24}(k)]^T$$
$$\bar{\boldsymbol{v}}_3(k) = [\bar{v}_{31}(k),\ \bar{v}_{32}(k)]^T$$
$$\bar{v}_{ij}(k) = T \sum_{l=k-(n-1)}^{k} \tilde{v}_{ij}(l), \text{ for } (i,j) = \{(1,3),\ (2,3),\ (3,1)\}$$
$$\bar{v}_{ij}(k) = T^2 \sum_{l=k-(n-1),\, m=l-(n-1)}^{k} \sum^{l} v_{ij}(m), \text{ for other } (i,j)$$
$$\tilde{v}_{13}(l) \equiv \varepsilon(l) - \varepsilon(l-(n-1))$$
$$\tilde{v}_{23}(l) \equiv \theta(l) - \theta(l-(n-1))$$
$$\tilde{v}_{31}(l) \equiv \phi(l) - \phi(l-(n-1))$$

Hence, the estimate model for (39) is given by

$$\hat{z}_i(k) = \hat{\boldsymbol{\zeta}}_i^T(k)\bar{\boldsymbol{v}}_i(k),\ i = 1,\ 2,\ 3 \tag{43}$$

and the system parameters $\hat{\boldsymbol{\zeta}}_i(k)$ can be identified from expression (43) without use of the velocities or accelerations of ε, θ and ϕ.
Finally, the following recursive least squares algorithm is applied to the estimate model (43).

$$\hat{\boldsymbol{\zeta}}_i(k) = \hat{\boldsymbol{\zeta}}_i(k-1) + \frac{P_i(k-1)\bar{\boldsymbol{v}}_i(k-1)\left[z_i(k-1) - \hat{z}_i(k-1)\right]}{\bar{\lambda}_i + \bar{\boldsymbol{v}}_i^T(k-1)P_i(k-1)\bar{\boldsymbol{v}}_i(k-1)} \tag{44}$$
$$P_i^{-1}(k) = \bar{\lambda}_i P_i^{-1}(k-1) + \bar{\boldsymbol{v}}_i(k-1)\bar{\boldsymbol{v}}_i^T(k-1)$$
$$P_i^{-1}(0) > 0\,, \quad 0 < \bar{\lambda}_i \leq 1,\ i = 1,\ 2,\ 3$$

Note here that the estimated velocity and acceleration signals are still used in the control input (19).

5.1.2 Experimental studies

The design parameters for the integral form of the identification algorithm are given by $n = 100$, $\bar{\lambda}_1 = \bar{\lambda}_2 = \bar{\lambda}_3 = 0.9999$ and ${P_1}^{-1}(0) = {P_2}^{-1}(0) = 10^3 I_4$, ${P_3}^{-1}(0) = 10^3 I_2$. The reference inputs u_{M1} and u_{M2} are given by

$$u_{M1} = \begin{cases} 0.3, & 45k - 30 \leq t < 45k - 7.5 \\ -0.1, & 45k - 7.5 \leq t < 45k + 15 \end{cases}$$
$$u_{M2} = \begin{cases} 0, & 0 \leq t < 7.5 \\ -0.8, & 45k - 37.5 \leq t < 45k - 22.5 \\ 0.8, & 45k - 22.5 \leq t < 45k \end{cases} \tag{45}$$
$$k = 0, 1, 2, \cdots$$

The other parameters are the same as those of the previous section.
The outputs are shown in Figs. 9 and 10. The tracking performance of both the outputs ε and ϕ is improved in comparison with the previous section. However, there remains a tracking error. The estimated parameters are plotted in Figs. 11 and 12. All of the parameters change slowly, and the variation of the estimated parameters in Figs. 11 and 12 is smaller than that of the corresponding value shown in Figs. 7 and 8.

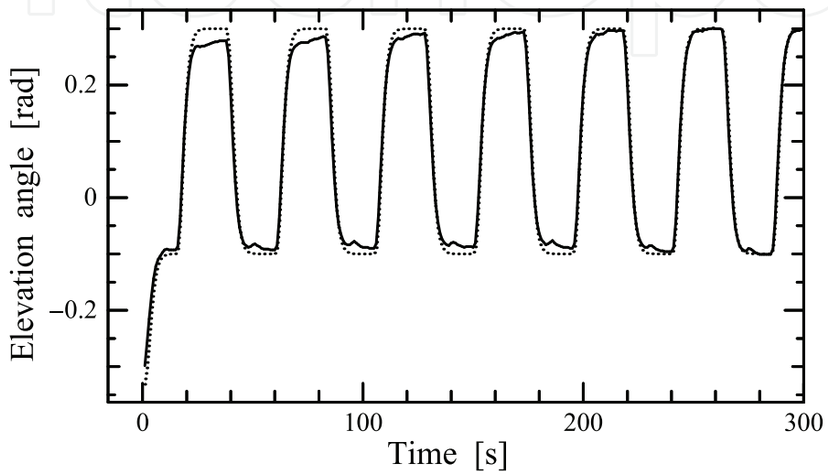

Fig. 9. Time evolution of angle ε (—) and reference output ε_M ($\cdots$).

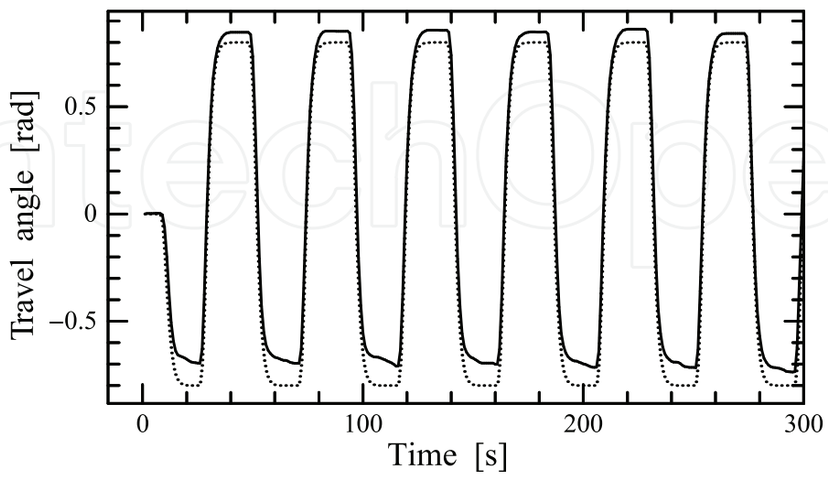

Fig. 10. Time evolution of angle ϕ (—) and reference output ϕ_M ($\cdots$).

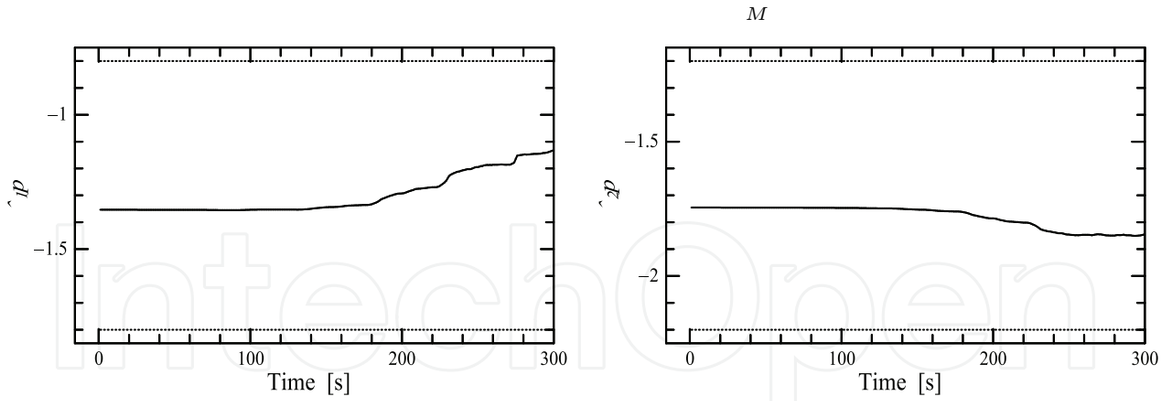

Fig. 11. Time evolution of the estimated parameters $\hat{p}_1$ and $\hat{p}_2$. The dotted lines represent the limited values of variation.

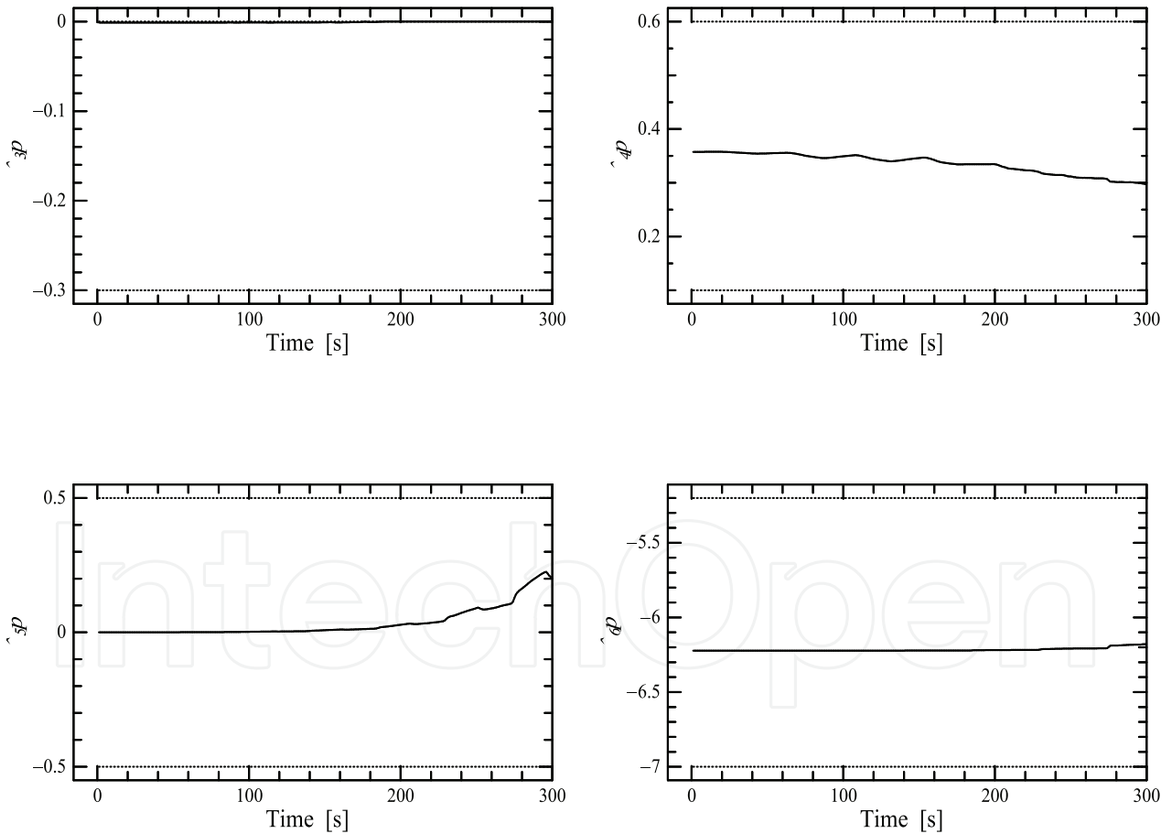

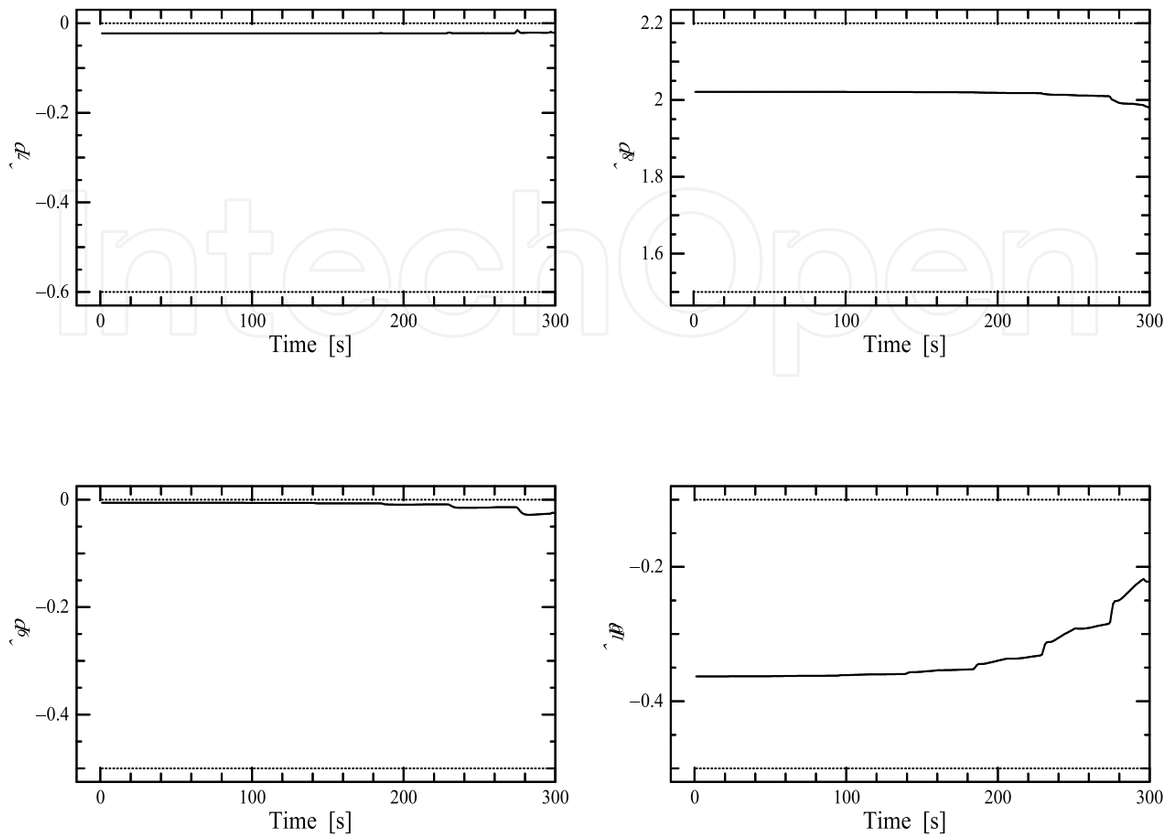

Fig. 12. Time evolution of the estimated parameters from $\hat{p}_3$ to $\hat{p}_{10}$. The dotted lines represent the limited values of variation.

5.2 The model equations with model uncertainties and external disturbances

5.2.1 Parameter identification algorithm

Although the use of the integral form of the dynamics has improved the tracking performance of both the outputs ε and θ, tracking errors still remain. On the basis that these errors are caused by model uncertainties and external disturbances, for example, motor dynamics or friction (other than viscous friction), we add the additional terms f_ε, f_θ and f_ϕ into equation (4) to represent model uncertainties and external disturbances. Generally, the additional terms should be given as, for instance,

$$f_\varepsilon(t) = \sum c_i f_i(t) \tag{46}$$

where c_i is a constant and f_i is a known function of time. For simplicity, however, here we assume these additional terms are constant because tracking errors in the experimental results approximately remain constant in Fig. 10. Then, the system dynamics are expressed as

$$w_1(k) \equiv \ddot{\varepsilon}(k) = \boldsymbol{\zeta}_1^T \boldsymbol{q}_1(k)$$
$$w_2(k) \equiv \ddot{\theta}(k) = \boldsymbol{\zeta}_2^T \boldsymbol{q}_2(k) \tag{47}$$
$$w_3(k) \equiv \ddot{\phi}(k) = \boldsymbol{\zeta}_3^T \boldsymbol{q}_3(k) \tag{48}$$

where

$$\begin{aligned}
\boldsymbol{\xi}_1 &= \left[\boldsymbol{\zeta}_1^T,\ p_{11}\right]^T \\
\boldsymbol{\xi}_2 &= \left[\boldsymbol{\zeta}_2^T,\ p_{12}\right]^T \\
\boldsymbol{\xi}_3 &= \left[\boldsymbol{\zeta}_3^T,\ p_{13}\right]^T \\
\boldsymbol{q}_1(k) &= \left[\boldsymbol{v}_1^T(k),\ 1\right]^T \\
\boldsymbol{q}_2(k) &= \left[\boldsymbol{v}_2^T(k),\ 1\right]^T \\
\boldsymbol{q}_3(k) &= \left[\boldsymbol{v}_3^T(k),\ 1\right]^T \\
p_{11} &= f_\varepsilon / J_\varepsilon \\
p_{12} &= f_\theta / J_\theta \\
p_{13} &= f_\phi / J_\phi
\end{aligned}$$

It is worth noting that all the parameters p_i $(i = 1, \ldots, 13)$ of the equations are constant. Then, the integral form of the dynamics is obtained as well as the previous subsection as

$$z_i(k) = \boldsymbol{\xi}_i^T \bar{\boldsymbol{q}}_i(k),\ i = 1,\ 2,\ 3 \tag{49}$$

where

$$\begin{aligned}
\bar{\boldsymbol{q}}_1(k) &= \left[\bar{\boldsymbol{v}}_1^T(k),\ \bar{q}_{15}(k)\right]^T \\
\bar{\boldsymbol{q}}_2(k) &= \left[\bar{\boldsymbol{v}}_2^T(k),\ \bar{q}_{25}(k)\right]^T \\
\bar{\boldsymbol{q}}_3(k) &= \left[\bar{\boldsymbol{v}}_3^T(k),\ \bar{q}_{33}(k)\right]^T \\
\bar{q}_{15}(k) &= T^2 \sum_{l=k-(n-1)}^{k} \sum_{i=l-(n-1)}^{l} 1 \\
&= T^2(n-1)^2 \\
\bar{q}_{25}(k) &= T^2(n-1)^2 \\
\bar{q}_{33}(k) &= T^2(n-1)^2
\end{aligned}$$

Hence, defining the estimated parameter vectors corresponding to the vectors $\boldsymbol{\xi}_1$, $\boldsymbol{\xi}_2$, $\boldsymbol{\xi}_3$ as $\widehat{\boldsymbol{\xi}}_1(k)$, $\widehat{\boldsymbol{\xi}}_2(k)$, $\widehat{\boldsymbol{\xi}}_3(k)$, the estimate model for expression (49) is given by

$$\widehat{z}_i(k) = \widehat{\boldsymbol{\xi}}_i^T(k)\bar{\boldsymbol{q}}_i(k), \quad i = 1,\ 2,\ 3 \tag{50}$$

and the system parameters $\widehat{\boldsymbol{\xi}}_i(k)$ can be identified by the following recursive least squares algorithm.

$$\begin{aligned}
\widehat{\boldsymbol{\xi}}_i(k) &= \widehat{\boldsymbol{\xi}}_i(k-1) + \frac{P_i(k-1)\bar{\boldsymbol{q}}_i(k-1)\left[z_i(k-1) - \widehat{z}_i(k-1)\right]}{\bar{\lambda}_i + \bar{\boldsymbol{q}}_i^T(k-1)P_i(k-1)\bar{\boldsymbol{q}}_i(k-1)} \\
P_i^{-1}(k) &= \bar{\lambda}_i P_i^{-1}(k-1) + \bar{\boldsymbol{q}}_i(k-1)\bar{\boldsymbol{q}}_i^T(k-1) \\
& \qquad P_i^{-1}(0) > 0\,, \quad 0 < \bar{\lambda}_i \leq 1,\ i = 1,\ 2,\ 3
\end{aligned} \tag{51}$$

5.2.2 Experimental studies

The weighting factor of the least squares algorithm is given by

$$\widetilde{\lambda} = 0.9995 + 0.0005 \exp\left(-5\sqrt{e_1^2 + e_2^2}\right)$$

The updating period of the parameters, T, is $T = 10$ [ms], while other design parameters are the same as those of the previous section. The value of T stated above led to the best experimental result unlike the previous experimental studies.
The outputs are depicted in Figs. 13 and 14, while the estimated parameters are shown in Figs. 15, 16 and 17. The tracking performance of both of the outputs ε and ϕ has been further improved by the inclusion of the uncertainties.

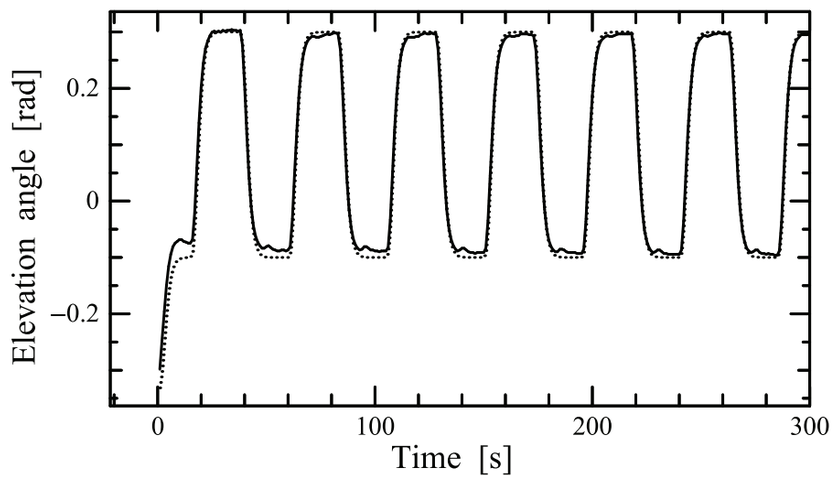

Fig. 13. Time evolution of angle ε (—) and reference output ε_M ($\cdots$).

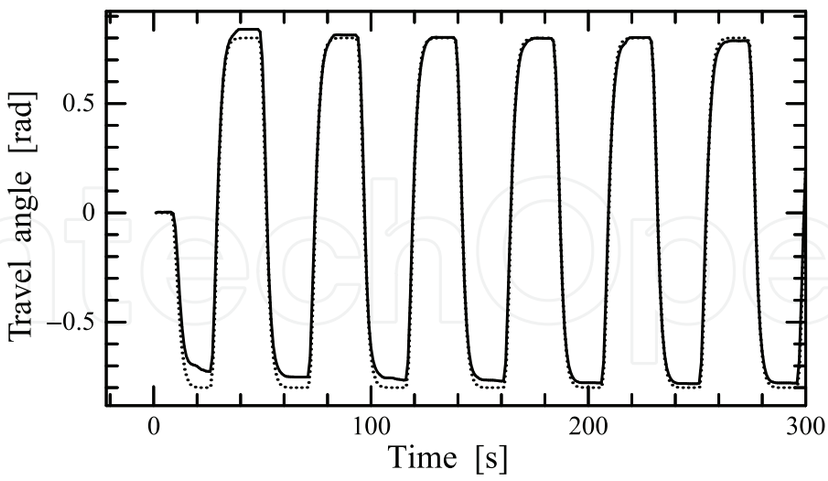

Fig. 14. Time evolution of angle ϕ (—) and reference output ϕ_M ($\cdots$).

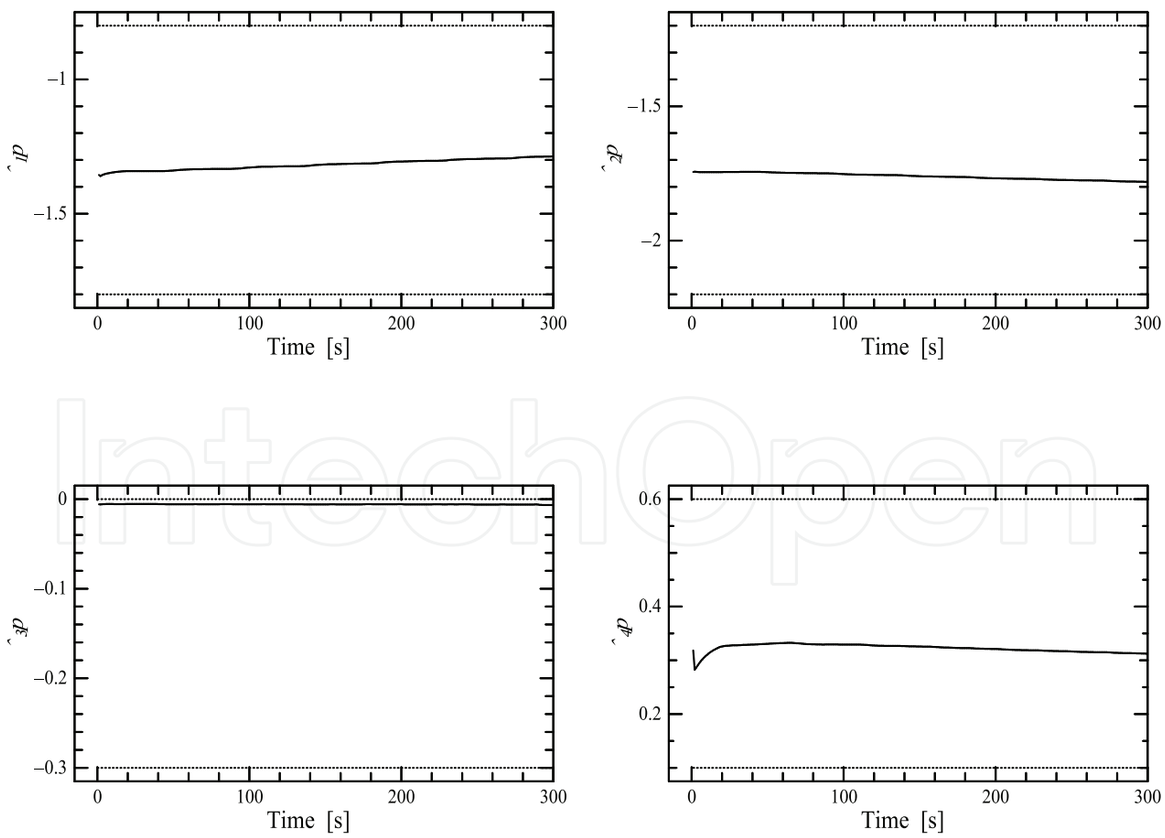

Fig. 15. Time evolution of the estimated parameters from $\hat{p}_1$ to $\hat{p}_4$. The dotted lines represent the limited values of variation.

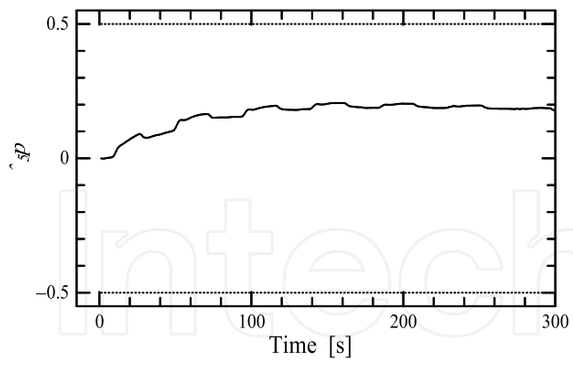
0.5
0
−0.5
0
100
200
300
Time [s]

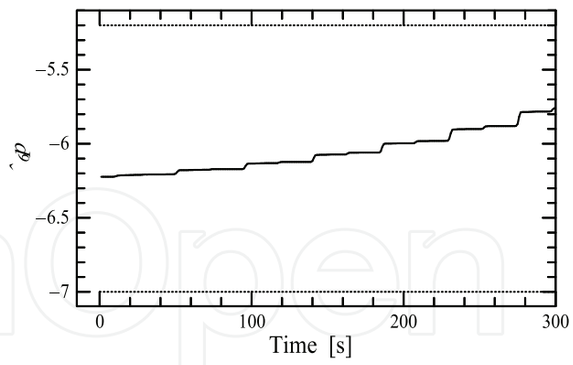
−5.5
−6
−6.5
−7
0
100
200
300
Time [s]

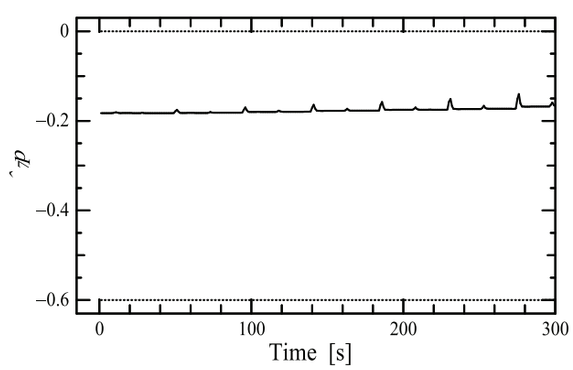
0
−0.2
−0.4
−0.6
0
100
200
300
Time [s]

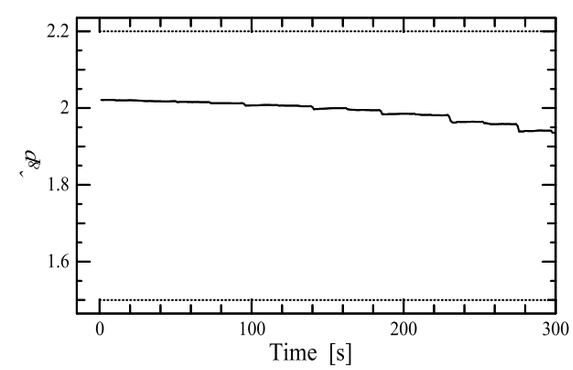
2.2
2
1.8
1.6
0
100
200
300
Time [s]

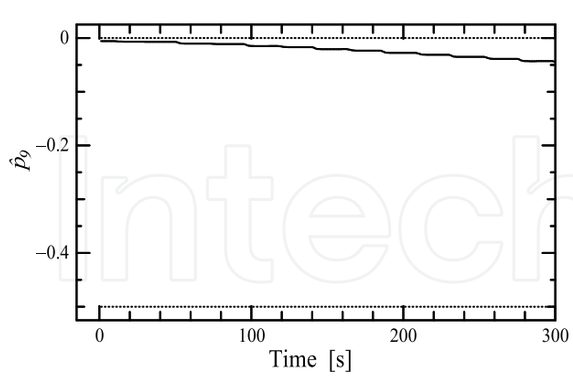
0
−0.2
−0.4
0
100
200
300
Time [s]

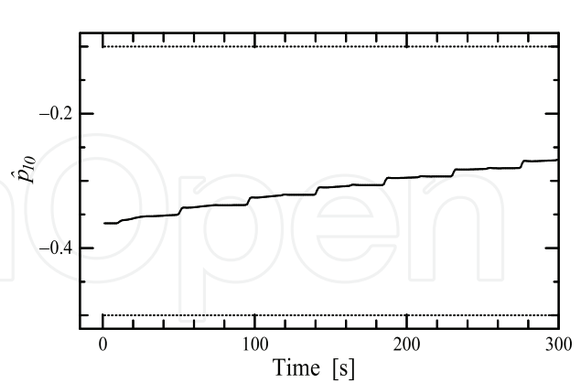
−0.2
−0.4
0
100
200
300
Time [s]

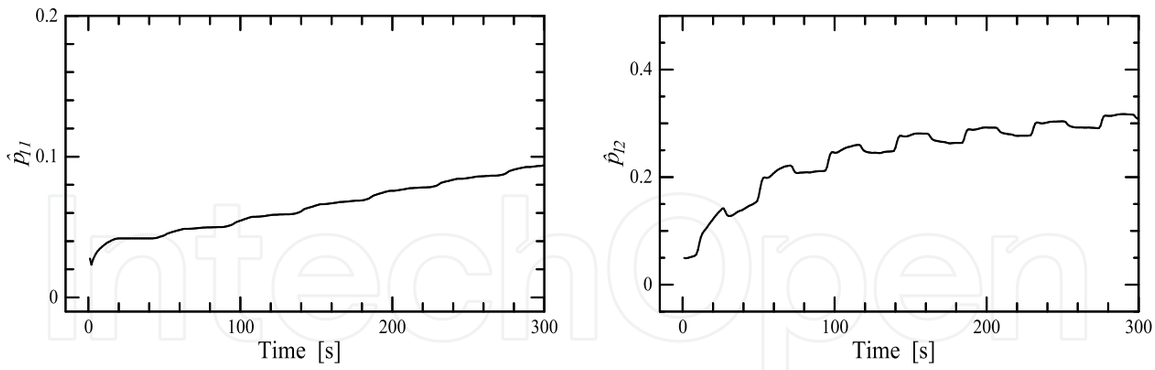

Fig. 16. Time evolution of the estimated parameters from $\hat{p}_5$ to $\hat{p}_{12}$. The dotted lines represent the limited values of variation.

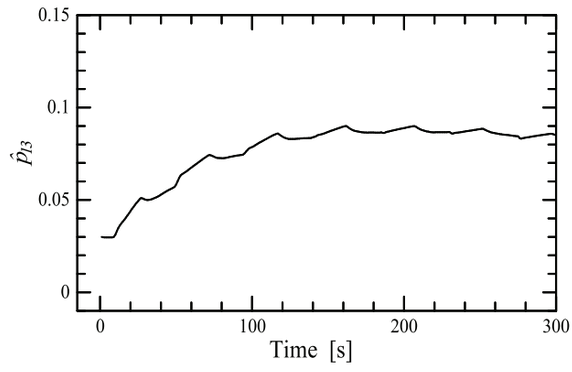

Q

Fig. 17. Time evolution of the estimated parameter $\hat{p}_{13}$. The dotted lines represent the limited values of variation.

6. Conclusions

This paper considers the nonlinear adaptive model following control of a 3-DOF model helicopter. The system model here is not decouplable by static state feedback, and the nonlinear structure algorithm is applied. When a simple model following controller is designed, it is not easy to obtain a good control performance mainly due to the parameter uncertainties. Then, two parameter identification schemes are discussed: The first scheme is based on the differential equation model. This scheme is unable to obtain a good tracking control performance because of the inaccuracy of the estimated velocity and acceleration signals. The second scheme is designed for a dynamics model derived by applying integral operators to the differential equations expressing the system dynamics. Hence, this identification algorithm requires neither velocity nor acceleration signals. The experimental results show that the second method yields a better tracking result, although tracking errors still remain. Finally, we introduce additional terms into the equations of motion to express model uncertainties and external disturbances. With reference to experimental results, this modification is shown to further improve the tracking control performance.

7. References

[1] Apkarian, J. (1998). 3D Helicopter experiment manual, Quanser Consulting, Inc
[2] Avila, J, C.; Brogliato, B.; Dzul, A. & Lozano, R. (2003). Nonlinear modelling and control of
helicopters, *Automatica*, Vol. 39, No. 9, pp. 1583-1596
[3] Isurugi, Y. (1990). Model following control for nonlinear systems, INRIA Reports, No.1332
[4] Kaloust, J.; Ham, C. & Qu, Z. (1997). Nonlinear autopilot control design for a 2-DOF helicopter
model, *IEE Proc. Control Theory and Appl.*, Vol. 144, No. 6, pp. 612-616
[5] Kutay, A, T.; Calise, A, J; Idan, M. & Hovakimyan, N. (2005). Experimental results on adaptive
output feedback control using a laboratory model helicopter, *IEEE Trans. Control Systems Technology*, Vol. 13, No. 2, pp. 196-202
[6] Sira-Ramirez, H.; Zribi, M. & Ahmad, S. (1994). Dynamical sliding mode control approach for
vertical flight regulation in helicopters, *IEE Proc. Control Theory and Appl.*, Vol. 141, No. 1, pp. 19-24
[7] Shima, M.; Isurugi, Y.; Yamashita, Y.; Watanabe, A.; Kawamura, T. & Yokomichi M. (1997).
Control Theory of Nonlinear Systems (in Japanese), Corona Publishing Co., Ltd.

IntechOpen

Mechatronic Systems Simulation Modeling and Control

Edited by Annalisa Milella Donato Di Paola and Grazia Cicirelli

ISBN 978-953-307-041-4
Hard cover, 298 pages
Publisher InTech
Published online 01, March, 2010
Published in print edition March, 2010

This book collects fifteen relevant papers in the field of mechatronic systems. Mechatronics, the synergistic blend of mechanics, electronics, and computer science, integrates the best design practices with the most advanced technologies to realize high-quality products, guaranteeing at the same time a substantial reduction in development time and cost. Topics covered in this book include simulation, modelling and control of electromechanical machines, machine components, and mechatronic vehicles. New software tools, integrated development environments, and systematic design methods are also introduced. The editors are extremely grateful to all the authors for their valuable contributions. The book begins with eight chapters related to modelling and control of electromechanical machines and machine components. Chapter 9 presents a nonlinear model for the control of a three-DOF helicopter. A helicopter model and a control method of the model are also presented and validated experimentally in Chapter 10. Chapter 11 introduces a planar laboratory testbed for the simulation of autonomous proximity manoeuvres of a uniquely control actuator configured spacecraft. Integrated methods of simulation and Real-Time control aiming at improving the efficiency of an iterative design process of control systems are presented in Chapter 12. Reliability analysis methods for an embedded Open Source Software (OSS) are discussed in Chapter 13. A new specification technique for the conceptual design of self-optimizing mechatronic systems is presented in Chapter 14. Chapter 15 provides a general overview of design specificities including mechanical and control considerations for micro-mechatronic structures. It also presents an example of a new optimal synthesis method to design topology and associated robust control methodologies for monolithic compliant microstructures.

InTech Europe
University Campus STeP Ri

InTech China
Unit 405, Office Block, Hotel Equatorial Shanghai

Slavka Krautzeka 83/A
51000 Rijeka, Croatia
Phone: +385 (51) 770 447
Fax: +385 (51) 686 166
www.intechopen.com

No.65, Yan An Road (West), Shanghai, 200040, China
中国上海市延安西路65号上海国际贵都大饭店办公楼405单元
Phone: +86-21-62489820
Fax: +86-21-62489821

IntechOpen

IntechOpen